J. Fluid Mech. (2024), *vol*. 982, A3, doi:10.1017/jfm.2024.61

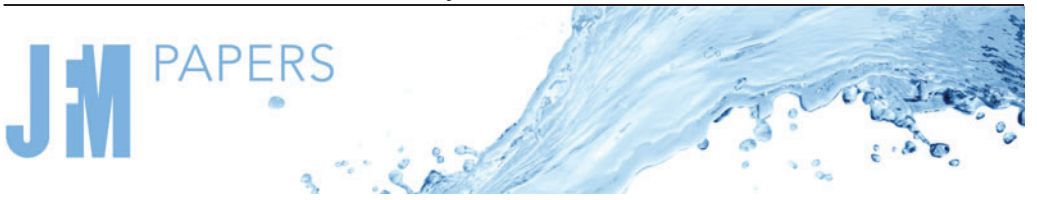

A simple prediction of time-mean and wave orbital velocities in submerged canopy

Xiaoxia Zhang[1,2,†], **Chuyan Zhao**[2] **and Heidi Nepf**[3]

[1]Water Science and Environmental Engineering Research Center, College of Chemical and Environmental Engineering, Shenzhen University, Shenzhen 518060, China

[2]State Key Laboratory of Coastal and Offshore Engineering, Dalian University of Technology, Dalian 116024, China

[3]Department of Civil and Environmental Engineering, Massachusetts Institute of Technology, Cambridge, MA 02139, USA

(Received 7 July 2023; revised 29 November 2023; accepted 8 January 2024)

Flow within submerged canopies influences the transport of nutrients, sediment, pollutants, plant seeds and the settlement of larvae. To improve our understanding of mass transport within canopies, a simple model is proposed to predict the total time-varying velocity within submerged rigid canopies (representing coral reefs) and flexible canopies (representing seagrasses and saltmarshes). The model divides the momentum equations into a canopy layer and free-stream layer. The difference in the time derivative of the velocity between the two layers is balanced by the sum of the shear stress and canopy drag, both of which depend on the in-canopy total velocity. The present model extended the shear stress model developed for steady current to combined current and wave conditions without additional calibrating coefficients. The model agreed well with the in-canopy velocity measured in the present and several previous studies. Importantly, the proposed model significantly improved the accuracy of canopy time-mean velocity prediction, which reduced the root mean square error by more than 50 %, compared with previous models. The model revealed that the addition of waves can significantly decrease the in-canopy time-mean velocity.

Key words: wave-structure interactions, coastal engineering, flow-structure interactions

1. Introduction

Submerged canopies are present in many aquatic ecosystems, including coral reefs, seagrass meadows as well as salt marshes and dwarf mangroves (during high tide and storm surge). These ecosystems serve multiple ecological and environmental functions.

† Email address for correspondence: xiaoxiazhang@szu.edu.cn

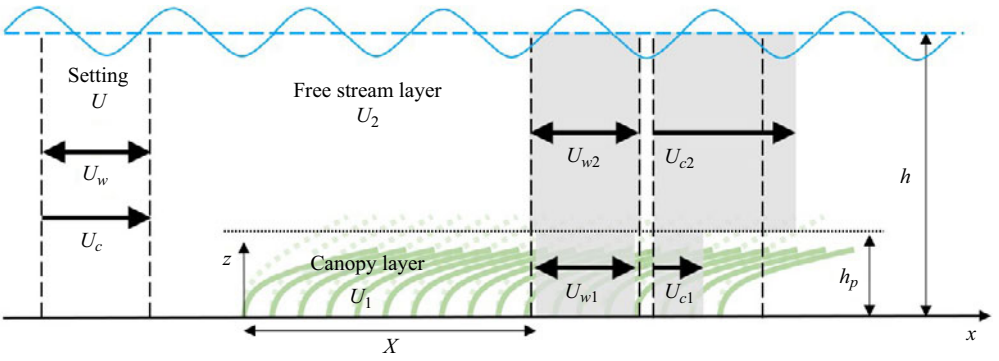

Figure 1. Illustration of velocity modification due to canopy resistance. Here, U_c is the imposed current and U_w is the wave orbital velocity defined upstream of the canopy. Subscripts 1 and 2 denote velocity in the canopy layer and in the free-stream layer above the canopy, respectively, h and h_p are the water depth and canopy height, respectively, X is the velocity adjustment length and δ is the penetration length describing the length scale of turbulent momentum exchange between the two layers.

For example, these canopies provide shelter, nursery habitat and food sources for fish (Costanza *et al*. 1997; Waycott, Longstaff & Mellors 2005; Whitfield 2017). They improve water quality by filtering nutrients (De Los Santos *et al*. 2020) and capturing suspended sediments (Palmer *et al*. 2004). The canopy resistance reduces current and waves, which reduces bed erosion and enhances coastal stability (Gedan *et al*. 2011).

The resistance of the canopy can significantly alter the flow structure and hydrodynamic properties within and above a submerged canopy (Villanueva *et al*. 2017). As illustrated in figure 1, when flow enters a submerged canopy with canopy height h_p, two distinct flow regions are formed, the in-canopy and above-canopy layer. Note that, for a flexible canopy, the effective canopy height is smaller than the fully erect plant height when plants move in response to hydrodynamic forces. Within the canopy layer, the horizontal velocity gradually decelerates from the leading edge due to canopy drag. This results in a deflection of flow into the above canopy layer, which causes an increase in the above-canopy velocity. Velocities within and above the canopy are referenced by subscripts 1 and 2, respectively. After an adjustment length X, the time-mean current reaches a new equilibrium, called the fully developed flow structure. The adjustment length X is inversely proportional to the canopy drag, C_Da, with C_D the drag coefficient and a the canopy density defined as the frontal area per canopy volume. Based on equation (10) in Chen, Jiang & Nepf (2013) and equation (5.1) in Lei & Nepf (2021), $X/h_p \approx 1$ to 20 for canopy density (defined as the plant frontal area per bed area) $ah_p = 0.1$ to 10, which is a typical range for submerged canopies, and the shallow submergence $2 < h/h_p < 5$, where h is the water depth.

The canopy velocity structure determines the transport of sediment, pollutants, pollen, plant seeds and fish larvae through submerged ecosystems (Falter, Atkinson & Merrifield 2004; Lowe, Koseff & Monismith 2005*b*; Reidenbach *et al*. 2006; Malul, Holzman & Shavit 2020; Huai *et al*. 2021; Stride *et al*. 2023). Further, for some hydrodynamic conditions, the physical mass transfer was found to control the nutrient uptake rate by submerged ecosystems (Falter *et al*. 2004; Larned, Nikora & Biggs 2004; Morris *et al*. 2008). For example, the ammonium uptake in *Cymodocea nodosa* meadow was twice that observed for a *Zostera noltii* meadow, which was attributed to a doubling of the in-canopy velocity (Morris *et al*. 2008). Hydrodynamic models that can accurately predict the in-canopy and above canopy velocity provide a useful tool to understand and quantify

the mass transfer and nutrient uptake in submerged ecosystems (Lowe *et al*. 2005*b*; Stride *et al*. 2023).

Previous studies have described the velocity field associated with submerged canopies for a uni-directional current in both the fully developed (Luhar & Nepf 2013) and the adjustment regions (Chen *et al*. 2013; Lei & Nepf 2021). For a deeply submerged canopy, defined as a water depth to canopy height ratio $h/h_p > 10$, the flow within the canopy is driven by the turbulent stress at the top of the canopy (Nepf 2012). For shallow submergence ($1 < h/h_p < 5$), canopy flow is driven by both the turbulent stress and potential gradients (Nepf 2012). Many canopies exist within the submergence range $1 < h/h_p < 5$. For example, seagrasses usually colonize water depths $1 < h < 10$ m (Duarte 1991), with canopy height $h_p = 0.1$ to 1 m (based on the blade length summarized in table 3 in Luhar *et al*. 2010 and table 1 in Hansen & Reidenbach 2012), corresponding to $1 < h/h_p < 100$. For many intertidal salt marshes, $h_p = 0.4$ to 0.9 m, with water depths in the range from $h = 0.8$ to 2 m, varying from an emergent to submerged state over a tide cycle with $1 < h/h_p < 5$ when submerged (e.g. Ysebaert *et al*. 2011; Garzon *et al*. 2019; Zhang *et al*. 2020).

The canopy resistance is often described by the dimensionless canopy density, ah_p (the plant frontal area per bed area). For many coastal canopies, e.g. salt marshes, seagrasses and mangroves summarized in Nepf (2012), $ah_p > 0.1$, indicating that the canopy drag is large compared with the bed drag and generates a shear layer with an inflection point near the top of the canopy. The in-canopy time-mean velocity U_{c1} is decreased and the above-canopy time-mean velocity U_{c2} is increased compared with the depth-averaged U_c (Chen *et al*. 2013; Lei & Nepf 2021). Specifically, the ratio of U_{c1} to U_c, defined as time-mean velocity reduction α_c, is significantly smaller than 1, i.e. $\alpha_c = U_{c1}/U_c \ll 1$ (figure 1). Theoretical models have been developed to predict the in-canopy and above canopy current velocity (Chen *et al*. 2013; Lei & Nepf 2021). For example, Chen *et al*. (2013) predicted the current velocity within an array of rigid cylinders based on the continuity and momentum equations within and above the canopy (1.1), herein noted as the CJN model after the authors' names

$$\alpha_c = \frac{U_{c1}}{U_c} = \frac{1}{1 - \dfrac{h_p}{h}\lambda_p + \sqrt{\dfrac{C_D a h_p}{2C(1-\lambda_p)}\left(\dfrac{h-h_p}{h}\right)^3}}, \tag{1.1}$$

in which $\lambda_p = V_p/h_p$ is the solid volume fraction within the canopy, V_p is the submerged plant volume per bed area and C characterizes the turbulent momentum exchange between the canopy and over-flow layers. Previous studies have suggested (Konings, Katul & Thompson 2012)

$$C = K_c\left(\frac{\delta}{h}\right)^{1/3}, \tag{1.2}$$

in which $K_c = 0.07 \pm 0.02$ (SD, standard deviation) is an empirical constant (Chen *et al*. 2013), δ is the penetration length that quantifies the vertical extent of the shear layer within the canopy. Chen *et al*. (2013) assumed $\delta = 0.23/(C_D a)$ for $h/h_p \geq 2$ and $\delta = 0.23(h/h_p - 1)/(C_D a)$ for $h/h_p < 2$. Recently, Lei & Nepf (2021) extended the CJN model to flexible canopies and to describe the evolution of velocity from the leading edge for both wide (two-dimensional) submerged canopies and submerged canopies of finite width (three-dimensional), referred to as the L&N model. The L&N model improved the parameterization of turbulent momentum exchange between the two layers by considering

the physical limits of the penetration length δ, which is constrained by the canopy height (h_p) and the depth of water above the canopy ($h - h_p$)

$$\delta = \min\left(\frac{0.3 \pm 0.1}{C_D a}, h - h_p, h_p\right). \tag{1.3}$$

Considering the relative magnitudes of the inertial and drag forces in a range of natural canopies, the reduction of the wave orbital velocity within the canopy is significantly less than the reduction of a uni-directional current (Lowe, Koseff & Monismith 2005*a*). As a result, waves are often more important than current for generating in-canopy fluid motion that enhances the nutrient uptake and mass transfer, e.g. within coral reefs (Hearn, Atkinson & Falter 2001; Falter *et al*. 2004, Falter, Atkinson & Coimbra 2005; Reidenbach *et al*. 2006) and seagrasses (Thomas & Cornelisen 2003). The reduction of the in-canopy wave orbital velocity has been described by a two-layer model (Lowe *et al*. 2005*a*), called the LKM model

$$\frac{\partial(U_{w1} - U_{w2})}{\partial t} = \frac{|U_{w2}|U_{w2}}{L_S} - \frac{|U_{w1}|U_{w1}}{L_D} - \frac{C_M \lambda_p}{1 - \lambda_p}\frac{\partial U_{w1}}{\partial t}, \tag{1.4}$$

in which $L_S = 2h_p/C_f$ is the shear length scale, $L_D = 2h_p(1 - \lambda_P)/(C_D a h_p)$ is the drag length scale, C_f is the friction coefficient for the canopy interface and C_M is the inertial force coefficient. Although Lowe *et al*. (2005*a*) considered waves with a background current in their experiments, (1.4) was derived for the wave component only. The reduction in the wave orbital velocity within the canopy is described by $\alpha_w^* = U_{w1}/U_{w2}$, i.e. the ratio of the wave orbital velocity for the two layers at the same x position. When inertial forces dominate, (1.4) reduces to

$$\alpha_w^* = \frac{U_{w1}}{U_{w2}} = \frac{(1 - \lambda_p)}{1 + (C_M - 1)\lambda_p}. \tag{1.5}$$

When the wave period is infinitely long, (1.4) approaches the unidirectional limit, for which a simplified solution for the time-mean velocity reduction is (Lowe *et al*. 2005*a*)

$$\alpha_c^* = \frac{U_{c1}}{U_{c2}} = \sqrt{\frac{L_D}{L_S}}. \tag{1.6}$$

Note that the LKM model defined the canopy velocity reduction relative to the velocity above the canopy, and a superscript * was added to distinguish this from the definition used in the CJN and L&N models, in which the canopy velocity reduction is defined relative to the imposed velocity unaffected by the canopy (U), i.e. $\alpha_c = U_{c1}/U_c$. With these definitions, $\alpha_c^* < \alpha_c$, because flow diverted from the canopy to the overflow layer results in $U_{c2} > U_c > U_{c1}$. To make comparisons between different models and with measurements from different studies, the reduction coefficients can be transformed considering the mass conservation through the canopy (equation 18 in Chen *et al*. 2013, see also (2.10) in the present study)

$$\alpha_c^* = \frac{\alpha_c(h - h_p)}{h - \alpha_c h_p(1 - \lambda_p)}. \tag{1.7}$$

For many natural canopies, the reduction in wave orbital velocity is in the range of $\alpha_w^* = 0.68$ to 0.99. The lowest values of α_w^* are associated with very dense canopies, e.g. rigid canopies with $D = 50$ mm and a density of 100 stems m^{-2} (Lowe *et al*. 2005*a*) or

$D = 6.4$ mm and a density of 3100 stems m^{-2} (van Rooijen *et al*. 2020). In comparison, the current ratio falls in the range of $\alpha_c^* = 0.03$ to 0.3, which is much smaller than the wave ratio, indicating that the time-mean current experiences a much greater reduction within a canopy compared with the wave velocity (Luhar *et al*. 2010). Further, submerged canopies are often exposed to combined current and waves. In these combined conditions, current and waves may affect one another, so that the in-canopy time-mean current and wave orbital velocity should be predicted together. As introduced above, the LKM model predicts current and wave orbital velocity reduction as two limits of behaviour with respect to wave excursion, and it cannot describe the interaction between currents and waves. The first effort to predict current and wave velocity together was made in Zeller *et al*. (2015). Specifically, they developed a one-dimensional Reynolds-averaged Navier–Stokes model, herein called the ZWK model

$$\frac{\partial U_1}{\partial t} + \frac{[UW]_{h_p}}{h_p} = -\frac{1}{\rho}\frac{\partial P}{\partial x} + \frac{\tau_{xz}|_{h_p}}{h_p} - \frac{1}{2}\frac{C_D a |U_1| U_1}{1-\lambda_p} - \frac{C_M \lambda_p}{1-\lambda_p}\frac{\partial U_1}{\partial t}, \tag{1.8}$$

in which U_1 and U_2 are the total velocity in the canopy and free-stream layer, respectively, W is the vertical velocity and P is pressure. The shear stress at the top of the canopy is modelled as $\tau_{xz}|_{h_p} = C_{Sm}^2 |U_2 - U_1|(U_2 - U_1)$, with C_{Sm} the Smagorinsky coefficient (Vreman, Geurts & Kuerten 1997). Assuming W follows linear wave theory, the vertical advection at the interface of the two flow layers is modelled as

$$\frac{[UW]_{h_p}}{h_p} = -\frac{(h-h_p)U_1 + h_p U_2}{h}\frac{1}{\rho\sqrt{gh}}\frac{\partial P}{\partial x}. \tag{1.9}$$

Equation (1.8) predicts the total time-varying in-canopy velocity U_1, which is the sum of time-mean U_{c1} and wave orbital U_{w1}, such that both α_c^* and α_w^* can be obtained. In the current limit, (1.8) reduces to

$$\alpha_c^* = \frac{\sqrt{\dfrac{L_D}{L_S'}}}{\sqrt{\dfrac{L_D}{L_S'}} + \sqrt{1 - \dfrac{h_p}{h}}}, \tag{1.10}$$

in which the shear length scale is defined by $L_S' \equiv h_p / C_{Sm}^2$. The difference between (1.10) and (1.6) comes from the fact that (1.10) considers the pressure gradient for unidirectional flow, which is neglected in the ZWK model (1.6).

Scale analysis shows that the ZWK model is only effective for a limited range of flow and canopy conditions. Specifically, the ZWK model (1.8) is applicable for $A_w/L_D \ll 10$, $L_D/L_S' \ll 1$, $U_c/U_w \sim O(1)$, $2 < h/h_p < 5$ and $Fr \ll 1$ (Zeller *et al*. 2015). Here, A_w is the wave orbital excursion and $Fr = \sqrt{(U_c^2 + U_w^2)/(gh)}$ is the Froude number. However, natural canopy and flow conditions can have a much wider range of parameters. First, U_c/U_w can vary between the current limit and wave limit, so that U_c/U_w can range from 0 to infinity. Further, some natural canopies, such as salt marshes, vary from emergent (during low tide) to submerged (during high tide or storm surge), such that a shallow submergence, $1 < h/h_p < 2$, is a common natural condition (Ysebaert *et al*. 2011; Zhang *et al*. 2020).

The present study developed a model for combined wave–current conditions to overcome the limitations of previous models. The new model is applicable to a much wider

Model name	Model prediction	Empirical coefficients	Reference
CJN model	$\alpha_c = f(a, \lambda_p, h_p, h, U_c)$	C_D, C	Chen *et al.* (2013)
L&N model	$\alpha_c = f(a, \lambda_p, h_p, h, U_c)$	C_D, C	Lei & Nepf (2021)
LKM model	$\alpha_c^* = f(a, \lambda_p, h_p)$ $\alpha_w^* = f(a, \lambda_p, h_p, U_{w2})$	C_D, C_M, C_f	Lowe *et al.* (2005*a*)
ZWK model	$\alpha_c^*, \alpha_w^* = f(a, \lambda_p, h_p, h, U_2)$	C_D, C_M, C_{Sm}	Zeller *et al.* (2015)

Table 1. Models predicting in-canopy velocity for fully developed canopy flow.

range of current and wave combinations, covers the limits of pure current and pure wave and can be applied to both rigid and flexible structures such as seagrasses and salt marshes. Experiments were conducted to measure detailed velocity profiles upstream of and within a submerged canopy formed of rigid cylinders under pure current, pure wave and combined current and wave conditions. The new model was validated using measurements in the present study as well as previous studies, including flexible seagrass and salt marsh plant models. The new model performed as well or better than previous models described in the literature (table 1).

2. Theoretical modelling

2.1. *Force on individual plant*

The impact of a canopy on the velocity field is described through the hydrodynamic drag generated by individual plants. Therefore, it makes sense to begin with a description of that drag. For greatest generality, we use a model that accounts for plant flexibility and morphology in both waves and current. Specifically, the drag force on a plant with multiple leaves (each is l_l long, b wide and d thick) distributed on a central stem (with diameter D and length l_s), F_d, has been described for both waves alone and in combination with current (Zhang & Nepf 2021*b*, 2022)

$$F_d = \underbrace{F_{r,l}\{C_s N_l K_l (Ca_l L_l)^{-1/4}\}}_{\textit{force on leaves}} + \underbrace{F_{r,s}\{K_s (Ca_s L_s)^{-1/4}\}}_{\textit{force on stem}}. \tag{2.1}$$

In (2.1), the time-varying drag forces on an individual rigid leaf ($F_{r,l}$) and a rigid stem ($F_{r,s}$) are modified by the bracketed terms that account for the reduction in drag due to leaf and stem reconfiguration. Throughout the manuscript, the subscripts l and s represent parameters associated with the leaves and stem, respectively, N_l is the number of leaves on the plant, C_s is the sheltering coefficient that reflects the drag reduction due to sheltering and interaction between leaves and stem and K_l and K_s are coefficients that reflect the geometric difference between a leaf (flat) and a stem (cylindrical). Specifically, based on measurements on an individual leaf, $K_l = 1$ (Lei & Nepf 2019*b*), and for a cylindrical stem $K_s = 1.2$ (Zhang, Lin & Nepf 2021). The Cauchy number, Ca, is the ratio of hydrodynamic drag to the restoring force due to structural stiffness, see (2.4). Here, L is the length ratio between the structure length, l, and wave orbital excursion, A_w, see (2.5)

$$F_{r,l} = \frac{1}{2}\rho C_{D,l} b l_l |U_1| U_1 + \rho C_{M,l} b d l_l \frac{\partial U_1}{\partial t}, \tag{2.2}$$

$$F_{r,s} = \frac{1}{2}\rho C_{D,s} D l_s |U_1| U_1 + \rho C_{M,s} \frac{\pi D^2}{4} l_s \frac{\partial U_1}{\partial t}, \tag{2.3}$$

$$Ca = \frac{\rho A U_{max}^2}{EI/l^2}, \tag{2.4}$$

$$L = \frac{l}{A_w}, \tag{2.5}$$

$$U_{max} = \max(|U_1|). \tag{2.6}$$

Here, U_{max} is the maximum in-canopy velocity. In (2.4), A is the frontal area, and $A = Dl_s$ for a cylindrical stem and $A = bl_l$ for a flat leaf, E is the Young's modulus, I is the second momentum of area and $I = \pi D^4/64$ for a cylindrical stem and $I = bd^3/12$ for a flat leaf.

Finally, flexible plants bend in response to flow, called reconfiguration, which reduces drag. The influence of plant flexibility on plant drag is captured by the scaling term $(Ca\,L)^{-1/4}$ (2.1), which applies to waves with $L > 1$ and $Ca\,L > 1$. For $Ca\,L < 1$, the drag reduction is negligible and $F_d = F_{r,l}\{C_s N_l K_l\} + F_{r,s} K_s$ (Luhar & Nepf 2016; Henderson 2019; Lei & Nepf 2019*b*; Zhang & Nepf 2021*a*). For pure current, the reconfiguration term $(Ca\,L)^{-1/4}$ in (2.1) is replaced by $Ca^{-1/3}$ (Luhar & Nepf 2011).

2.2. *Fully developed in- and above-canopy velocity*

The fully developed in- and above-canopy velocities are defined for $x > X$. Beyond this position, the time-mean velocity does not adjust further with increasing x, but the wave orbital velocity might decrease due to plant-induced wave energy dissipation. For simplicity, the evolution of the wave velocity with distance was not considered in the present model, which focused on the vertical adjustment of horizontal velocity in response to canopy drag. Consider a co-linear current U_c and wave U_w that enter the canopy at $x = 0$. The total imposed velocity is defined as the depth-averaged velocity over $z = 0$ to h (figure 1)

$$U = U_c + U_w \cos(\phi), \tag{2.7}$$

in which ϕ is the wave phase. After an adjustment length of X, the flow structure is fully developed, with a reduced in-canopy time-mean current U_{c1} and wave orbital velocity U_{w1}, compared with the velocity in the absence of a canopy (without energy dissipation), which equals the imposed velocity U_c and U_w. The above-canopy time-mean current U_{c2} is increased. The degree of velocity reduction in the canopy is represented by α_c^* and α_w^* (figure 1). Assuming there is no phase difference in the vertical direction, the total in-canopy (defined as the depth average over $z = 0$ to h_p) and above-canopy (defined as the depth average over $z = h_p$ to h) velocities are, respectively,

$$U_1 = U_{c1} + U_{w1} \cos(\phi), \tag{2.8}$$

$$U_2 = U_{c2} + U_{w2} \cos(\phi). \tag{2.9}$$

Conservation of mass requires that, at each phase of the wave, the sum of flux within each layer equals the depth-averaged flux, expressed as

$$U(\phi)h = U_1(\phi)h_p(1 - \lambda_p) + U_2(\phi)(h - h_p). \tag{2.10}$$

Assume the bottom friction can be neglected relative to the canopy drag (i.e. $ah_p > 0.1$), and the free-surface stress is zero, then the vertically averaged momentum equation in the

canopy layer (2.11) and the overflow layer (2.12) are, respectively,

$$\frac{\partial U_1(\phi)}{\partial t} + \frac{W_1(\phi)U_1(\phi)}{h_p} + U_1(\phi)\frac{\partial U_1(\phi)}{\partial x} = -\frac{1}{\rho}\frac{\partial P_1(\phi)}{\partial x} + \frac{\tau_{xz}|_{h_p}}{h_p} - \langle F_d(\phi)\rangle, \quad (2.11)$$

$$\frac{\partial U_2(\phi)}{\partial t} + \frac{W_2(\phi)U_2(\phi)}{h - h_p} + U_2(\phi)\frac{\partial U_2(\phi)}{\partial x} = -\frac{1}{\rho}\frac{\partial P_2(\phi)}{\partial x} - \frac{\tau_{xz}|_{h_p}}{h - h_p}. \quad (2.12)$$

The bracket notation $\langle\rangle$ defines the average drag over the canopy. Integrating the continuity equation over the canopy layer, $W_1(\phi) = -h_p(\partial U_1(\phi)/\partial x)$. Substituting for W_1 in (2.11), the convective terms cancel. Similarly, in the overflow layer, $W_2(\phi) = -(h - h_p)(\partial U_2(\phi)/\partial x)$, and the convective terms cancel. The convective terms were also neglected in previous layer-averaged models (Lowe *et al*. 2005*a*; Weitzman *et al*. 2015; Jacobsen 2016). The pressure gradients are associated with the time-mean free-surface slope, which is hydrostatic, and the surface wave dynamic pressure. For shallow-water waves ($kh \ll 1$), the dynamic pressure is $\rho g a_w \cos(\phi)$ (Lin 2008) and does not depend on the vertical position, such that $\partial P_1(\phi)/\partial x = \partial P_2(\phi)/\partial x$. Based on field measurements, e.g. data shown in Garzon *et al*. (2019), Zhang *et al*. (2020) and Zhang, Lin & Chen (2022*a*), offshore and coastal regions are often dominated by shallow to near shallow wave conditions with $kh = 0.1$ to 1. Considering shallow submergence, $h/h_p \geq 2$, the estimated pressure gradient for the canopy and free-stream layers differed by 20 % at maximum based on linear wave theory with finite water depth (Lin 2008). Therefore, for simplicity, $\partial P_1(\phi)/\partial x = \partial P_2(\phi)/\partial x$ was considered in the model derivation and the model is theoretically valid for $kh \leq 1$.

For N_s plants per bed area, the total canopy resistance per unit in-canopy fluid can be calculated from the force on an individual plant, $F_d(\phi)$. Specifically, $\langle F_d(\phi)\rangle = (1/\rho)(F_d(\phi)N_s/h_p(1 - \lambda_p))$. Using this and combining (2.11) and (2.12)

$$\frac{\partial U_2}{\partial t} - \frac{\partial U_1}{\partial t} = \frac{1}{\rho}\frac{F_d N_s}{h_p(1 - \lambda_p)} - \frac{h}{h_p(h - h_p)}\tau_{xz}|_{h_p}. \quad (2.13)$$

To simplify the notation, the phase ϕ will be dropped, but keep in mind that each term varies with the wave phase. The plant drag F_d is a function of in-canopy velocity U_1. The shear stress, $\tau_{xz}|_{h_p}$, is a function of the velocity difference $U_2 - U_1$. For combined current and wave conditions, we assume that the shear stress model developed for a unidirectional current is valid at each velocity phase, i.e.

$$\tau_{xz} = C|U_2 - U_1|(U_2 - U_1), \quad (2.14)$$

in which C characterizes the turbulent momentum exchange between the two layers (1.2). Solving (2.10), $U_2 = RU + R_1U_1$ with $R = h/(h - h_p)$, $R_1 = h_p(1 - \lambda_p)/(h - h_p)$ and plugging U_2 into (2.13), we obtained U_1 as a function of U

$$R_1\frac{\partial U}{\partial t} - (R_2 + 1)\frac{\partial U_1}{\partial t} = \frac{1}{\rho}\frac{F_d N_s}{h_p(1 - \lambda_p)} - \frac{R_1}{h_p}C|R_1U - (R_2 + 1)U_1|(R_1U - (R_2 + 1)U_1). \quad (2.15)$$

Since F_d is a function of U_1 and plant properties (2.1), the only unknown variable, U_1, can be solved by (2.13) when U_2 is known, or by (2.15) when U is known. The predicted total velocity is then separated into a time-mean U_{c1} and wave orbital velocity U_{w1}, which were used to quantify the velocity reduction parameters. For pure current, the time derivative is zero, and (2.15) reduces to (1.1), described by the CJN and L&N models (Chen *et al*. 2013; Lei & Nepf 2021). With waves, (2.13) and (2.15) need to be solved numerically. The associated MATLAB code is described in the supplementary material available at https://doi.org/10.1017/jfm.2024.61.

Flow condition	Cylinder (stem)	Flat plate (leaf)
Pure current	$C_{D,s} = 1 + 10Re_c^{2/3}$ $Re_c = \frac{U_1 D}{\upsilon}\frac{1-\lambda_p}{1-\sqrt{2\lambda_p/\pi}}$ Etminan, Lowe & Ghisalberti (2017)	$C_{D,l} = 1.95 + \frac{50}{Re}$ $Re = \frac{U_1 b}{\upsilon}$ Ellington (1991)
Waves, with or without current	$C_{D,s} = \begin{cases} 16\mathrm{KC}^{-0.52} & \mathrm{KC} \le 10 \\ \max(1.95,\ 10\mathrm{KC}^{-1/3}) & \mathrm{KC} > 10 \end{cases}$ Figure A1 in Zhang, Lin & Nepf (2022*b*)	$C_{D,l} = \begin{cases} 0.19\mathrm{KC} + 0.2 & \mathrm{KC} \le 11 \\ 7.6\mathrm{KC}^{-0.5} & 11 < \mathrm{KC} \le 25 \\ \max(1, 2.9\mathrm{KC}^{-0.2}) & \mathrm{KC} > 25 \end{cases}$ Figure A1 in Zhang *et al.* (2022*b*)

Table 2. Drag coefficient C_D and inertia coefficient C_M.

2.3. *Model coefficients*

The inertia coefficient was set to $C_M = 2$ for all conditions. The drag coefficient, C_D, was estimated from formulations described in the literature for pure current and pure wave conditions, as summarized in table 2. For pure waves, C_D was determined by the Keulegan–Carpenter number (KC) (Keulegan & Carpenter 1958), with $\mathrm{KC} = U_{max}T_w/D$ for cylinders and $\mathrm{KC} = U_{max}T_w/b$ for a flat plate with b the plate width. The wave drag model was also applied for the combined current and wave conditions. Although Keulegan & Carpenter (1958) only considered pure wave conditions in their experiments, previous studies have shown that the C_D dependence on KC also fits combined current and wave conditions, if KC is defined using the maximum horizontal velocity $U_{max} = \max(|U_1|)$ ((2.6), for combined current and waves) instead of the wave orbital velocity ($U_{max} = U_\mathrm{w}$ for pure waves). Specifically, the drag coefficient shown in table 2 correctly predicted the drag force measured on individual plants under combined current and waves (Zhang & Nepf 2022), and also predicted the measured wave dissipation by vegetation under the influence of current (Zhang & Nepf 2021*a*). Drag coefficients were taken from figure A1 in Zhang, Lin & Nepf (2022*b*), but with an adjustment for submergence needed to account for the reduction in drag at the free end of a cylinder, i.e. at the top of a rigid canopy (e.g. see figure 7 and equation 18 in Ghisalberti & Nepf 2004). Specifically, for the array geometry considered, the canopy average drag coefficient was reduced by a factor of 0.64 compared with that of an infinite cylinder (Ghisalberti & Nepf 2004). The measured in-canopy velocity was used to predict C_D, such that, for each case, different models applied the same drag coefficient. When provided in the references, the reported drag coefficients were used for validation, as in Lowe *et al.* (2005*a*) and Zeller *et al.* (2015). A 20 % uncertainty in C_D was assumed for all model predictions.

In addition to C_D and C_M, the LKM model requires a friction coefficient C_f to describe the turbulent momentum exchange between layers. Poggi *et al.* (2004) fitted friction factors for submerged arrays in the range of $C_f = 0.005$ to 0.13. Similarly, Luhar & Nepf (2013) showed that $C_f = 0.04$ works well in predicting their canopy flow observations, and Lowe *et al.* (2005*a*) found $C_f = 0.017$ to 0.032. Based on these studies, we assumed $C_f = 0.03 \pm 0.02$ in the LKM model to predict the velocity reduction and its uncertainty. Finally, the ZWK model requires a Smagorinsky coefficient C_{Sm}, which is suggested to fall between 0.1 and 0.2 (Vreman *et al.* 1997). Consequently, $C_{Sm} = 0.15 \pm 0.05$ was applied in the ZWK model in this study. Finally, for flexible canopies, h_p was assumed to be the mean deflected canopy height (see table S1 in the supplementary material).

3. Laboratory measurements of canopy flow velocity

To validate the proposed model, flume experiments were conducted in a 22 m long and 45 cm wide flume in the State Key Laboratory of Coastal and Offshore Engineering in Dalian University of Technology. For simplicity, the experiment used rigid cylinders with 6 mm diameter and 20 cm height distributed in a staggered array. The test canopy was 4 m long and filled the flume width. Three densities were considered, 284, 444 and 830 cylinders per bed area. The water depth was 40 cm, such that $h/h_p = 2$. Eight pure current, seven pure wave and sixteen combined current and wave conditions were used. See all tested combinations of canopy and flow conditions in table S1 in the supplementary material.

The leading edge of the canopy was designated as $x = 0$, with x positive in the streamwise direction. Velocity profiles with 4 mm vertical resolution were measured using a Nortek Vectrino profiler at $x = -0.2$, 0, 0.1, 0.3, 0.5, 0.7, 1, 1.5, 2, 3 m in the flume centre. The measurements in the canopy were taken at the middle of two adjacent cylinders both in the streamwise and channel width direction. At each position, the velocity was sampled at 100 Hz for 1 min. For each measurement, the horizontal velocity u for conditions with waves was separated into phase bins and despiked using the same method as in Zhang & Nepf (2022). The phase-averaged velocity was defined as the mean velocity in each phase bin, $\breve{u}(\phi, z)$. The depth-averaged velocity U was defined by the average of $\breve{u}(\phi, z)$ at $x = -1$ m over $z = 0$ to 30 cm. Based on profiles measured along the canopy, we determined that the flow was fully developed at $x = 3$ m. Using the profile at this position, U_1 was defined as the depth average of $\breve{u}(\phi, z)$ over the canopy height ($z = 0$ to 20 cm), and U_2 was defined as the depth average of $\breve{u}(\phi, z)$ above the canopy ($z = 20$ to 30 cm). Note that U (also U_1 and U_2) vary with wave phase, and the mean over all phase defines the time-mean velocity U_c and $U - U_c$ is the unsteady wave component. The wave orbital velocity is defined by the root mean square value, $U_w = \sqrt{(2/T_w)\int_0^{2\pi} (U - U_c)^2 \,\mathrm{d}\phi}$. From the baseline measurements without a canopy and measured at $x = -0.2$ and 1 (each case includes 160 measurements from $z = 0$ to 30 cm), the time-mean velocity at different z has an average uncertainty of 5 % (represented by the standard deviation). The associated uncertainties in the current and wave reduction were within 0.1 for all conditions (see table S1 in the supplementary material for details).

Data from several previous studies were used to extend the model validation to flexible canopies and canopy flow with a wider range of parameters. The detailed canopy and flow conditions of all sources of data are summarized in table S1 in the supplementary material. The canopy and flow conditions covered a wide range, $ah_p = 0.13$ to 1.36, $h/h_p = 1.3$ to 4.3, $L_D/L_S = 0.04$ to 0.34, $A_w/L_D = 0.04$ to 0.37, $U_c/U_w = 0.4$ to 7 (for combined current and wave conditions) and $Fr = 0.02$ to 0.21.

4. Result

4.1. *Time-mean in-canopy velocity under pure current*

Measured time-mean velocities under pure current conditions were compared with several models in the literature and with the new model. We consider the time-mean current reduction α_c ($= U_{c1}/U_c$) (figure 2*a*). Remember that the model proposed in the present study, (2.15), reduces to the L&N model for pure current conditions. The LKM model (1.6) and ZWK model (1.10) predicted α_c^* ($= U_{c1}/U_{c2}$) which was converted to α_c using (1.7). The L&N (green diamonds) and CJN (black triangles) models had the best agreement with measurements for both the rigid (open symbols) and flexible canopies (filled symbols),

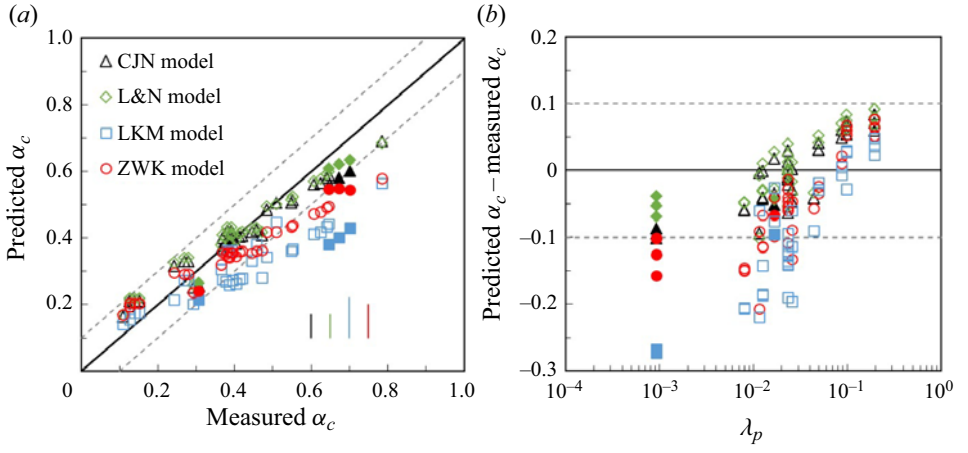

Figure 2. Comparison of model predictions with laboratory measurements with (*a*) predicted α_c plotted against measured α_c, (*b*) the error in prediction plotted against the canopy solid volume fraction. The open symbols and the filled symbols represent measurements within the present and previous rigid (Lowe *et al*. 2005*a*; Chen *et al*. 2013) and flexible canopies (Lei & Nepf 2021; Zhang & Nepf 2021*a*), respectively. The measurements have an uncertainty from 0.01 to 0.06 (see table S1 in the supplementary material). In (*a*), the vertical line with black, green, blue and red colours indicate the mean uncertainties in the predictions made by the CJN, L&N, LKM and ZWK models based on the uncertainty in the model empirical coefficients, respectively. The reference line for predicted α_c equalling measured α_c is shown by the black line with the dashed lines indicating an uncertainty of 0.1.

with the root mean square error (RMSE) = 0.05. The ZWK (red circles) and LKM (blue squares) models tended to predict greater reductions to the in-canopy velocity, i.e. lower values of α_c, except for the most dense canopies, producing the smallest α_c. Specifically, for seven cases from Lowe *et al*. (2005*a*) and three cases from Chen *et al*. (2013), each associated with $\lambda_p = 0.09$ to 0.2 (all other cases ranged within $\lambda_p < 0.05$), the LKM model had a slightly better agreement with the measurements (figure 2*b*). Over all the cases, RMSE for ZWK and LKM model were 0.09 and 0.14, respectively, which were significantly larger than the L&N and CJN model. The value of α_c can also be predicted through the full ZWK model (1.8) with a long wave period and a constant $U_2 = U_{c2}$. The α_c predictions by (1.8) were very close to the LKM model (not shown because it would collapse with the LKM model), but do not collapse to their simple prediction (1.10), which raises doubt in the LKM model (1.8) in capturing the limit of pure current conditions. This will be further supported by the comparison with combined current and wave conditions (figure 3 and the next section).

4.2. *Time-mean in-canopy velocity under combined current and waves*

Under combined wave and current conditions, the present model (2.13) is validated against $\alpha_c^* = U_{c1}/U_{c2}$ measured in previous (Lowe *et al*. 2005*a*; Zeller *et al*. 2015) and the present rigid canopies and for canopies of flexible marsh plants (Zhang & Nepf 2021*a*). Here, α_c^*, is used instead of α_c, because Lowe *et al*. (2005*a*) and Zeller *et al*. (2015) only reported α_c^* and the LKM and ZWK models predict α_c^*. Although our model was derived with a shallow-water wave assumption ($kh < 1$, water depth/wavelength $< 1/(2\pi)$ in practice), waves in coastal regions and flumes are usually associated with shallow to intermediate-water depths. Respecting this, the model was cautiously validated over a range of shallow to intermediate wave conditions, with $kh = 0.26$ to 1.83.

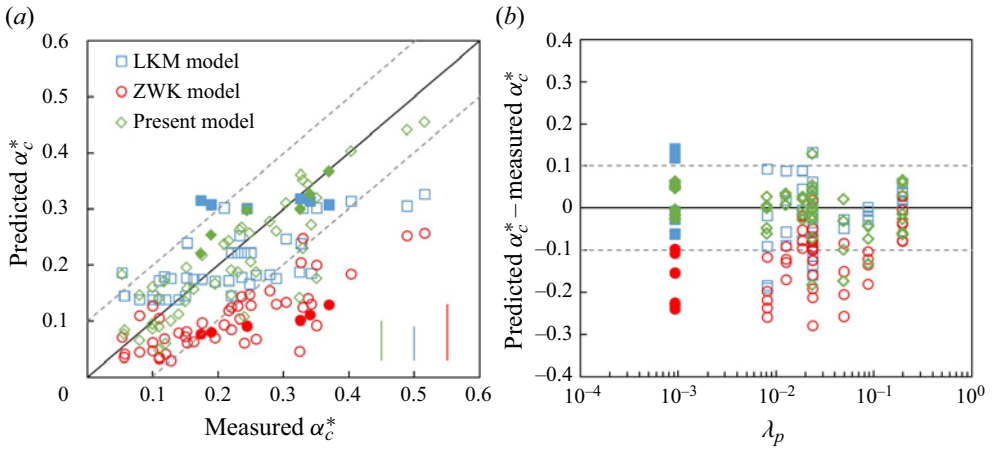

Figure 3. Comparison of model predictions and laboratory measurements with (*a*) predicted α_c^* plotted against measured α_c^* in rigid (open symbols) and flexible canopies (filled symbols), (*b*) difference between predicted and measured α_c^* versus canopy solid volume fraction λ_p. Vertical lines with green, blue and red colours indicate the mean uncertainty in the prediction made, respectively, by the present model (2.13), LKM and ZWK models. The solid black line shows perfect agreement, and the dashed lines indicate an error of 0.1. The uncertainty in each measurement is listed in table S1 in the supplementary material.

As shown in figure 3(*a*), the present model (2.13) captured the variation of in-canopy time-mean velocity under different canopy and flow conditions, with RMSE = 0.06. The LKM model predicted similar reductions for a given canopy structure, even though the measured α_c^* varied significantly with changing flow condition. The ZWK model did well for dense canopies with a large reduction in velocity and small α_c^*, but the discrepancy increased with increasing α_c^*, i.e. when canopy density decreased. The larger discrepancy in the ZWK model with lower canopy density (λ_p) is also shown in figure 3(*b*). The accuracies of the present model and the LKM model have no clear dependence on canopy density. Considering all cases, RMSE = 0.09 and 0.15 for the LKM and ZWK models, respectively, which were 1.5 and 2.5 times larger than the new model. It is worth noting that the new model worked well for both the rigid canopies (open symbols) and flexible canopies (filled symbols), and for a wide range of canopy density ($\lambda_p = 0.0009$ to 0.2).

4.3. *Reduction of wave orbital velocity within the canopy*

Figure 4(*a*) shows the comparison of measured and predicted reduction in wave orbital velocity for 52 combined current and wave cases (the same cases in figure 3) and 16 pure wave conditions (13 cases from the present study and 3 from Zhang & Nepf 2021*a*). For all conditions, the present model (2.13) predicted a similar wave orbital velocity to the LKM model, but the ZWK model was slightly deviated; RMSE = 0.13 for all the three models. Note that the LKM model predicted current and wave orbital velocities separately, without considering their mutual influence. As a result, for the same canopy, the LKM model predicted the same reduction in time-mean current under different flow conditions (figures 2 and 3). In contrast, the present model and the ZWK model predicted the time-varying total velocity. The ZWK model generally overestimated the measured reduction in time-mean velocity (smaller α_c, see figures 2 and 3), even considering the suggested range of Smagorinsky coefficient ($C_{Sm} = 0.1$ to 0.2 based on Vreman *et al.* 1997). The present model predicted a similar wave orbital velocity to previous models.

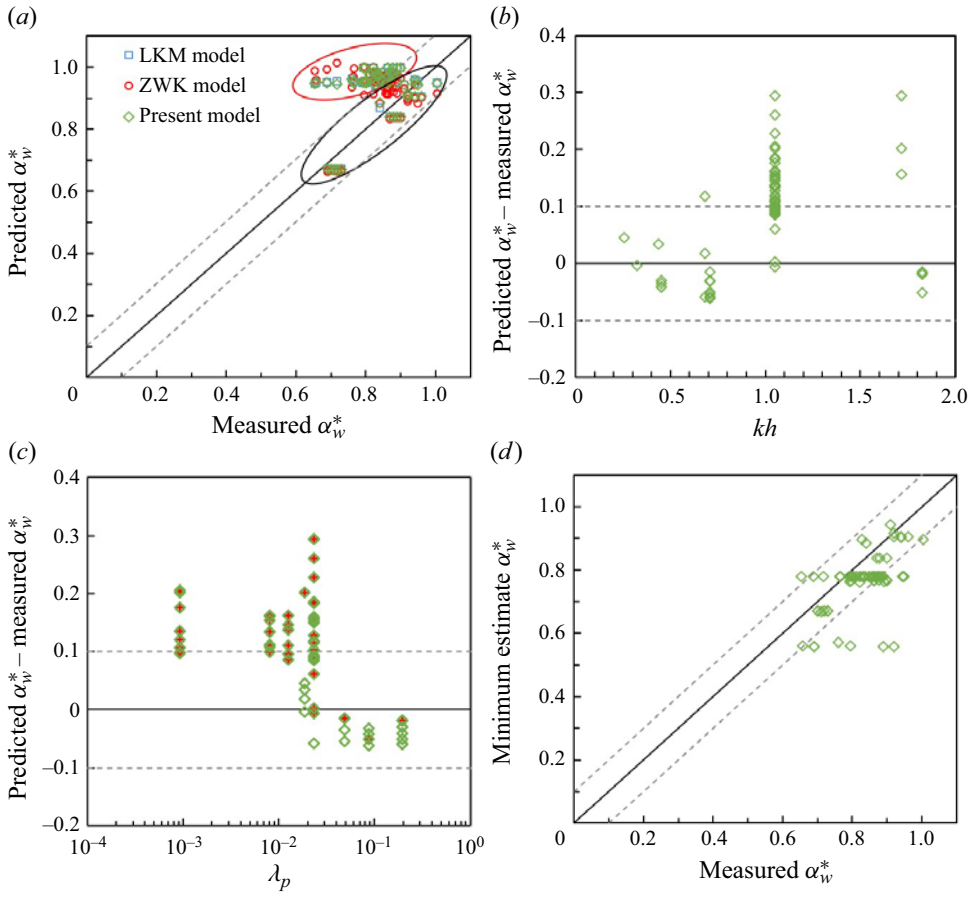

Figure 4. (*a*) Comparison of predicted and measured α_w^*. The LKM model and the present model predicted similar wave orbital velocity reductions, so that the symbols overlaps. The uncertainty in measured α_w^* ranged from 0.01 to 0.14. The uncertainty in predicted α_w^* is 0.001 (0.03) on average (maximum). (*b*,*c*) Show the error in the predicted α_w^* by the present model against the dimensionless wavenumber kh and canopy solid volume fraction λ_p, respectively. In (*c*), the symbols filled with red plus signs indicate cases with $kh > 1$ ($kh = 1.05$ to 1.83). (*d*) Compares the minimum α_w^* estimated by the present model and the linear wave theory with the measured α_w^*. The reference line for predicted α_w^* equalling measured α_w^* is shown by the black line with the dashed lines indicating an uncertainty of 0.1.

Considering the small difference between the models, the model performance will be discussed using the present model prediction.

From figure 4(*a*), the model performance can be separated into two regimes, the black oval indicates cases for which predicted α_w^* agreed with the measurements within uncertainty, and the red oval indicates cases for which the predicted $\alpha_w^* \approx 1$, while the measured α_w^* ranged from 0.66 to 0.9. The two distinct regimes of model performance can be explained by the fact that, in the absence of a canopy, the model assumed a depth-uniform velocity profile. This assumption works better for shallow-water waves ($kh < 1$, see figure 4*b*). For intermediate waves, $kh = 1.05$ to 1.83 (noted by red plus signs in figure 4*c*), the wave orbital velocity is greater near the surface and smaller near the bed, even in the absence of a canopy, which caused the measured α_w^* to deviate from the model assumptions, contributing to poor agreement between the measured and predicted values.

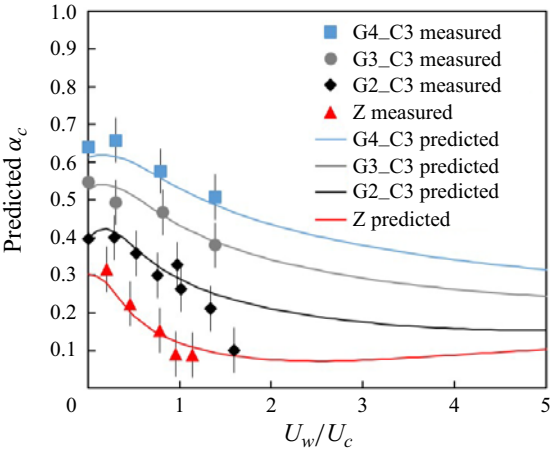

Figure 5. Reduction in time-mean current within the canopy, α_c over a range of wave velocities for canopy and current conditions labelled as G2–C3 ($N_s = 830$ stems m^{-2}), G3–C3 ($N_s = 444$ stems m^{-2}), G4–C3 ($N_s = 284$ stems m^{-2}) with $D = 6$ mm, $h_p = 0.2$ m, $h = 0.4$ m, $U_c = 16.3$ cm s^{-1} and Z ($N_s = 595$ stems m^{-2}, $D = 6.3$ mm, $h_p = 0.155$ m, $h = 0.4$ m, $U_c = 17.4$ cm s^{-1}). See table S1 in the supplementary material for detailed conditions. The symbols are measured values, and solid curves are predictions made by the present model (2.15). Error bars indicate an uncertainty of 0.06 in the measured α_c. The prediction has an average uncertainty of 0.03.

The impact of this discrepancy was greatest when the canopy had a small impact on wave velocity, i.e. for sparse canopies. Whereas for dense canopies (e.g. $\lambda_p \geq 0.05$), associated with a larger reduction in wave orbital reduction (figure 4*c*), the lack of a non-uniform reference state was less important, and agreement between model and prediction improved. Considering all conditions in figure 4, the ratio of wave orbital velocity averaged over the canopy layer ($z = 0$ to h_p) to that averaged over the free-stream layer ($z = h_p$ to h) ranged from 0.56 to 0.99 based on linear wave theory. Consistent with this, the minimum estimated α_w^* using the linear wave theory and the model prediction (2.13) agreed better with the measured α_w^* (figure 4*d*), with the RMSE reduced to 0.1. In conclusion, figure 4 suggests that the present model does well predicting the wave orbital velocity for shallow or near shallow waves $kh < 1$. However, for $kh > 1$, the non-uniform wave velocity in the absence of a canopy should be considered and corrected. Further research might be needed to improve the prediction of α_w^* for $kh > 1$. Note that the time-mean velocity predicted by the present model (2.13) agreed with measurements for all validated flow conditions ($kh = 0.26$ to 1.83).

4.4. *Effect of waves on the in-canopy time-mean velocity*

Measurements and the new model (2.15) were used to explore how waves affect the reduction of in-canopy current, i.e. α_c. For the same current and canopy conditions, the measured α_c decreased as the wave velocity (specifically U_w/U_c) increased (figure 5, symbols). That is, adding waves increased the drag experienced by the current. Equation (2.15), shown with solid curves in figure 5, captured this trend, and also suggested a limit of α_c. Specifically, the model predicted a minimum α_c is reached at $U_w/U_c = 2$ to 4, and further increases in wave velocity did not change α_c further. Importantly, figure 5 illustrates that the present model worked equally well in the pure current limit ($U_w = 0$) and for combined current and waves. It is worth noting that, although the model was

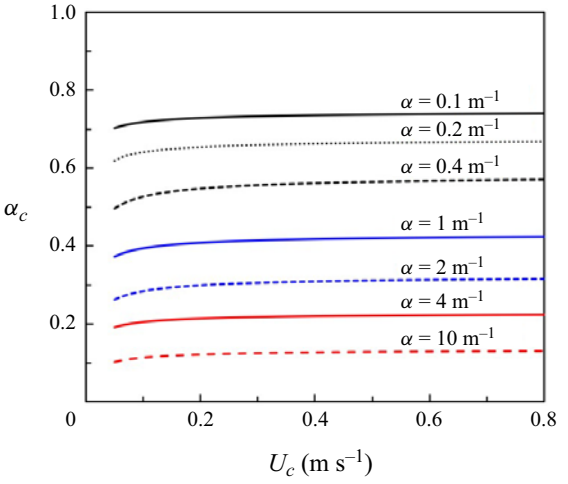

Figure 6. Variation of α_c with canopy density $a = N_s D_s = 0.1$ to 10 m^{-1} under pure current with increasing U_c. Curves in black, blue and red colours associated with $D = 2$, 5 and 10 mm, respectively. Predictions were made by the L&N model.

derived for a current with shallow-water waves ($kh < 1$), the predicted time-mean velocity agreed with measurements over a wider range of wavenumber ($kh = 0.26$ to 1.83) and the model performance was not affected by wavenumber. The decrease in α_c associated with increasing U_w can be explained through the plant drag. Specifically, for combined current and waves, the mean drag on a single rigid plant scales as $F_d \sim U_c^2 + 0.5U_w^2$, which becomes increasingly greater than $F_d \sim U_c^2$ as the wave velocity increases (Lei & Nepf 2019*a*; Tan & Yuan 2022). Greater mean canopy resistance resulted in greater in-canopy time-mean velocity reduction (smaller α_c).

5. Discussion

5.1. *Influence of canopy and flow condition on the current reduction*

First, the L&N model was used to explore the variation of time-mean reduction over sparse to dense canopies composed of rigid cylinders ($a = N_s D = 0.1$ to 10 m^{-1}), which covered the range of coastal vegetation canopies (Mullarney & Henderson 2018) under pure current ($U_c = 0.05$ to 0.8 m s^{-1}). For this test, the plant height $h_p = 1$ m and water depth $h = 2$ m. The prediction suggested that, for a given canopy and submergence, the time-mean reduction is the same within uncertainty (± 0.03) for $U_c = 0.05$ to 0.8 m s^{-1} (figure 6). The small uncertainty was caused by the dependence of α_c on canopy velocity through the drag coefficient C_D. Considering all tested conditions, the drag coefficient equation for rigid cylinders in a canopy (table 2) estimated C_D ranged from 1.7 to 1.1, while U_c increased from 0.05 to 0.8 m s^{-1}, which resulted in the same α_c within uncertainty (± 0.03). Considering the small uncertainty in α_c with changing current magnitude, a constant $C_D = 1.2$ (which is the average value for the tests shown in figure 6) and fixed setting current $U_c = 0.2$ m s^{-1} will be applied in the following discussion, so that the dependence of α_c on wave orbital velocity and canopy density can be highlighted. Note that, considering a 20 % uncertainty, $C_D = 1.2$ also represents the drag coefficient for the tested current and wave conditions shown in figure 7, based on the drag coefficient equation in table 2.

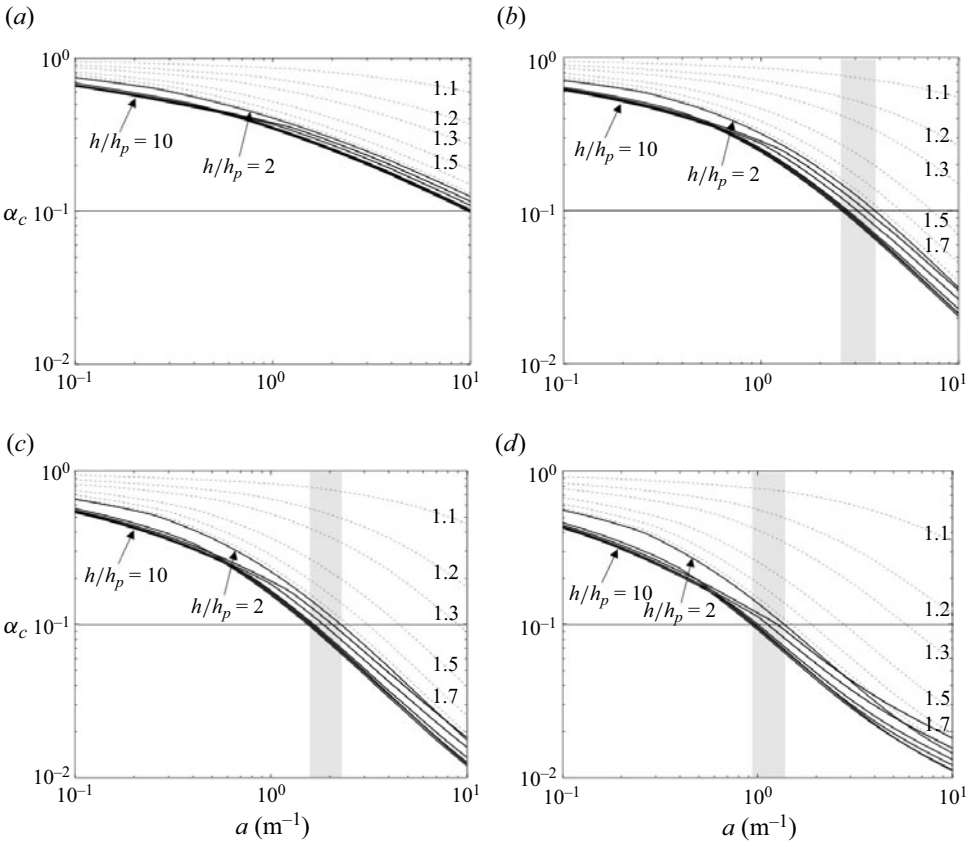

Figure 7. Time-mean velocity reduction versus the canopy density, $a = N_s D$ with $N_s = 50$ to 1000 cylinders per unit bed area and $D = 2$ to 10 mm, for (*a*) $U_w = 0$ m s^{-1}, (*b*) $U_w = 0.1$ m s^{-1}, (*c*) $U_w = 0.2$ m s^{-1} and (*d*) $U_w = 0.4$ m s^{-1}. Setting current velocity, wave period and water depth as constants, $U_c = 0.2$ m s^{-1}, $T_w = 4$ s, $h = 2$ m (corresponding to $kh = 0.77$). Each panel contains plant submergence from $h/h_p = 1.1$ to 10, indicated by the numbers. Predictions were made by the proposed model (2.15).

Under pure current, the time-mean velocity was reduced by a factor α_c, which decreased with increasing canopy density a, reaching $\alpha_c = 0.1$ for canopy density $a = 10$ m^{-1} (figure 7*a*). When waves were added, a reduction ratio of $\alpha_c = 0.1$ was reached at a lower canopy density. Specifically, $\alpha_c = 0.1$ was reached at $a = 3.0 \pm 0.8$ m^{-1}, $a = 2.0 \pm 0.3$ m^{-1} and $a = 1.0 \pm 0.2$ m^{-1}, as the waves increased over $U_w/U_c = 0.5$, 1 and 2, respectively (indicated by the grey area in figure 7). That is, the canopy density required to obtain $\alpha_c = 0.1$ was reduced by an order of magnitude when the wave orbital velocity was double the magnitude of the current. The value $a = 1$ m^{-1} is present in many natural canopies (e.g. those summarized in Nepf 2012; Zhang *et al.* 2022*b*), suggesting that, when waves are present, canopy time-mean velocity can be significantly reduced compared with pure current conditions. Next, consider the influence of the submergence ration. For $h/h_p = 2$ to 10, the degree of submergence had very little influence on canopy velocity, the solid black curves in figure 7. However, for smaller submergence, i.e. for $1 < h/h_p < 2$, α_c changed rapidly with decreasing h/h_p (dash curves in figure 7).

5.2. *Model performance and uncertainty*

We proposed a two-layer model to predict the in-canopy time-mean and wave orbital velocities. The momentum exchange between the layers was assumed to follow a shear stress model developed for pure current (proportional to $(U_2 - U_1)^2$). Specifically, for conditions with waves, the turbulent stress at each phase is assumed to be dominated by the instantaneous shear, such that the shear stress model $\tau_{xz} = C|U_2 - U_1|(U_2 - U_1)$ can be applied at each velocity phase. Consistent with this, the scale coefficient ($C = K_c(\delta/h)^{1/3}$) validated for pure current works well for general flow conditions. The canopy drag is estimated by a simple plant force model that can be applied for both flexible (e.g. salt marshes and seagrasses) and rigid structures. The model ((2.13) and (2.15)) prediction agreed with measured time-mean and wave orbital velocity reductions in both rigid (Lowe *et al*. 2005*a*; Chen *et al*. 2013; Zeller *et al*. 2015) and flexible canopies (Lei & Nepf 2021; Zhang & Nepf 2021*a*) within uncertainty. Considering a 20 % uncertainty in the drag coefficient and the uncertainties in the momentum exchange coefficient C, the proposed model has a maximum model uncertainty of ± 0.1 for current reduction and $\pm$ 0.01 for the wave orbital velocity reduction, respectively. The wave orbital velocity reduction coefficient is not sensitive to the empirical coefficients. By considering mass conservation, we have extended the canopy flow to the small submergence regime ($1 < h/h_p < 2$) and validated for a flexible salt marsh canopy with $h/h_p = 1.3$. This is important because many coastal canopies are within this submergence range; salt marshes are typical examples, as they may vary from emergent to submerged over each tide cycle.

The present model has been shown to work well for both the pure current and pure wave limits, as well as combined current and wave conditions. The model significantly improved the accuracy in predicting canopy time-mean flow with the influence of waves compared with exist models. The current model effectively captures the wave orbital velocity reduction for shallow-water waves with $kh < 1$. For deeper-water waves ($kh > 1$), we recommend the wave velocity profile without a canopy should also be considered.

5.3. *Model extension to N layer canopies*

Although the present model has been evaluated over a wide range of canopy and flow conditions, we cautiously recall that natural canopies are more complex, with varying structures and geometries and even multiple layers. For example, many mangroves (e.g. *Rhizophora* mangroves) have three typical layers, including the near bed dense root layer, the middle tree trunk layer and the upper crown layer. Further, the solid volume fraction of aquatic vegetation can vary vertically, e.g. figure 2 in Ysebaert *et al*. (2011) and figure 1(*e*) in Zhang *et al.* (2022*a*), such that a two-layer model might not reflect the vertical variation of velocity. The present model can be easily extended to an N-box model, as done in Zeller *et al*. (2015). Specifically, (2.13) can be extended to the following form:

$$\frac{\partial U_i}{\partial t} - \frac{\partial U_{i-1}}{\partial t} = \frac{1}{\rho}\frac{N_s}{h_p(1-\lambda_p)}F_{d,i-1} - \frac{\Delta_{z,i} + \Delta_{z,i-1}}{\Delta_{z,i}\Delta_{z,i-1}}\tau_{xz,i-1/2}, \tag{5.1}$$

in which $i = 1$ to N represents the flow layers from the bottom to the free surface and $\Delta_{z,i}$ is the thickness of the ith layer. The corresponding momentum exchange coefficient C becomes a function of the drag generated by the relevant layer and the penetration length is confined by the layer thickness.

6. Conclusion

The present study proposed a simple and robust prediction for fully developed canopy flow. The model was shown to accurately capture the reduction of in-canopy time-mean and wave orbital velocities under pure current, pure waves and combined current and wave conditions (figures 2 to 5). Specifically, the maximum uncertainty was $\pm$ 0.1 and $\pm$0.01 for α_c and α_w, respectively. Under pure current, the present model reduces to the prediction proposed by Lei & Nepf (2021). In comparison with the LKM model and the ZWK model, the present model had better agreement with laboratory measurements without any additional calibration. The model was validated for a wide range of conditions relevant to natural canopies: $ah_p = 0.13$ to 1.36; $h/h_p = 1.3$ to 4.3; $L_D/L_S = 0.04$ to 0.34; $A_w/L_D = 0.04$ to 0.37; $U_c/U_w = 0.4$ to 7 (for combined current and wave conditions) and $Fr = 0.02$ to 0.21.

With a simple force prediction for flexible plants from Zhang & Nepf (2021*b*, 2022), the present model ((2.13) and (2.15)) can be applied to both rigid canopies (e.g. coral reefs and mangroves) and flexible canopies (e.g. salt marshes and seagrasses). Although we focused on the fully developed regime, the model can be extended to describe the evolution at the canopy leading edge, following Lei & Nepf (2021). The proposed model can be coupled to large-scale, shallow-water numeric models (e.g. Maza, Lara & Losada 2013), to resolve the vertical velocity variation associated with submerged canopies. Finally, the canopy velocity prediction can be used within one-dimensional wave dissipation models (Lei & Nepf 2019*b*; van Veelen, Karunarathna & Reeve 2021; Zhang & Nepf 2021*a*) to improve the prediction of canopy drag.

Supplementary material. Supplementary material is available at https://doi.org/10.1017/jfm.2024.61.

Acknowledgements. This study was supported by the National Key Research and Development Program of China (no. 2022YFE0136700). Any opinions, findings and conclusions in this paper are those of author(s) and do not necessarily reflect the views of the National Key Research and Development Program of China.

Declaration of interests. The authors report no conflict of interests.

Author ORCIDs.
Xiaoxia Zhang https://orcid.org/0000-0002-2184-4208.

Author contributions. X.Z. designed the research, conducted the experiments, developed the theory, performed the simulation and data analysis, wrote the draft manuscript; C.Z. contributed to the experiments; H.N. contributed to the data analysis and theory development; All the authors reviewed and edited the manuscript.

References

Chen, Z., Jiang, C. & Nepf, H. 2013 Flow adjustment at the leading edge of a submerged aquatic canopy. *Water Resour. Res.* **49** (9), 5537–5551.

Costanza, R., d'Arge, R., de Groot, R., Farberl, S., Grassot, M., Hannon, B., Limburg, K., Naeem, S. & O'Neilltt, R.V. 1997 The value of the world's ecosystem services and natural capital. *Nature* **387** (15), 253–260.

De Los Santos, C.B., *et al.* 2020 Seagrass meadows improve inflowing water quality in aquaculture ponds. *Aquaculture* **528**, 735502.

Duarte, C.M. 1991 Seagrass depth limits. *Aquat. Bot.* **40** (4), 363–377.

Ellington, C.P. 1991 Aerodynamics and the origin of insect flight. In *Advances in Insect Physiology*, vol. 23, pp. 171–210. Elsevier.

Etminan, V., Lowe, R.J. & Ghisalberti, M. 2017 A new model for predicting the drag exerted by vegetation canopies. *Water Resour. Res.* **53**, 3179–3196.

FALTER, J.L., ATKINSON, M.J. & COIMBRA, C.F.M. 2005 Effects of surface roughness and oscillatory flow on the dissolution of plaster forms: evidence for nutrient mass transfer to coral reef communities. *Limnol. Oceanogr.* **50** (1), 246–254.

FALTER, J.L., ATKINSON, M.J. & MERRIFIELD, M.A. 2004 Mass-transfer limitation of nutrient uptake by a wave-dominated reef flat community. *Limnol. Oceanogr.* **49** (5), 1820–1831.

GARZON, J.L., MAZA, M., FERREIRA, C.M., LARA, J.L. & LOSADA, I.J. 2019 Wave attenuation by Spartina saltmarshes in the Chesapeake Bay under storm surge conditions. *J. Geophys. Res.: Oceans* **124** (7), 5220–5243.

GEDAN, K.B., KIRWAN, M.L., WOLANSKI, E., BARBIER, E.B. & SILLIMAN, B.R. 2011 The present and future role of coastal wetland vegetation in protecting shorelines: answering recent challenges to the paradigm. *Clim. Change* **106** (1), 7–29.

GHISALBERTI, M. & NEPF, H.M. 2004 The limited growth of vegetated shear layers. *Water Resour. Res.* **40**, 7.

HANSEN, J. & REIDENBACH, M. 2012 Wave and tidally driven flows in eelgrass beds and their effect on sediment suspension. *Mar. Ecol. Prog. Ser.* **448**, 271–287.

HEARN, C., ATKINSON, M. & FALTER, J. 2001 A physical derivation of nutrient-uptake rates in coral reefs: effects of roughness and waves. *Coral Reefs* **20** (4), 347–356.

HENDERSON, S.M. 2019 Motion of buoyant, flexible aquatic vegetation under waves: simple theoretical models and parameterization of wave dissipation. *Coast. Engng* **152**, 103497.

HUAI, W., LI, S., KATUL, G.G., LIU, M. & YANG, Z. 2021 Flow dynamics and sediment transport in vegetated rivers: A review. *J. Hydrodyn.* **33** (3), 400–420.

JACOBSEN, N.G. 2016 Wave-averaged properties in a submerged canopy: energy density, energy flux, radiation stresses and Stokes drift. *Coast. Engng* **117**, 57–69.

KEULEGAN, G.H. & CARPENTER, L.H. 1958 Forces on cylinders and plates in an oscillating fluid. *J. Res. Natl Bur. Stand.* **60** (5), 423.

KONINGS, A.G., KATUL, G.G. & THOMPSON, S.E. 2012 A phenomenological model for the flow resistance over submerged vegetation. *Water Resour. Res.* **48**, 2.

LARNED, S.T., NIKORA, V.I. & BIGGS, B.J.F. 2004 Mass-transfer-limited nitrogen and phosphorus uptake by stream periphyton: a conceptual model and experimental evidence. *Limnol. Oceanogr.* **49** (6), 1992–2000.

LEI, J. & NEPF, H. 2019*a* Blade dynamics in combined waves and current. *J. Fluids Struct.* **87**, 137–149.

LEI, J. & NEPF, H. 2019*b* Wave damping by flexible vegetation: connecting individual blade dynamics to the meadow scale. *Coast. Engng* **147**, 138–148.

LEI, J. & NEPF, H. 2021 Evolution of flow velocity from the leading edge of 2-D and 3-D submerged canopies. *J. Fluid Mech.* **916**, A36.

LIN, P. 2008 *Numerical Modeling of Water Waves*. Taylor & Francis.

LOWE, R.J., KOSEFF, J.R. & MONISMITH, S.G. 2005*a* Oscillatory flow through submerged canopies: 1. Velocity structure. *J. Geophys. Res.: Oceans* **110**, C10.

LOWE, R.J., KOSEFF, J.R. & MONISMITH, S.G. 2005*b* Oscillatory flow through submerged canopies: 2. Canopy mass transfer. *J. Geophys. Res.* **110** (C10), C10017.

LUHAR, M., COUTU, S., INFANTES, E., FOX, S. & NEPF, H. 2010 Wave-induced velocities inside a model seagrass bed. *J. Geophys. Res.: Oceans* **115**, C12.

LUHAR, M. & NEPF, H.M. 2011 Flow-induced reconfiguration of buoyant and flexible aquatic vegetation. *Limnol. Oceanogr.* **56** (6), 2003–2017.

LUHAR, M. & NEPF, H.M. 2013 From the blade scale to the reach scale: a characterization of aquatic vegetative drag. *Adv. Water Resour.* **51**, 305–316.

LUHAR, M. & NEPF, H.M. 2016 Wave induced dynamics of flexible blades. *J. Fluids Struct.* **61**, 20–41.

MALUL, D., HOLZMAN, R. & SHAVIT, U. 2020 Coral tentacle elasticity promotes an out-of-phase motion that improves mass transfer. *Proc. R. Soc. B: Biol. Sci.* **287** (1929), 20200180.

MAZA, M., LARA, J.L. & LOSADA, I.J. 2013 A coupled model of submerged vegetation under oscillatory flow using Navier–Stokes equations. *Coast. Engng* **80**, 16–34.

MORRIS, E.P., PERALTA, G., BRUN, F.G., VAN DUREN, L., BOUMA, T.J. & PEREZ-LLORENS, J.L. 2008 Interaction between hydrodynamics and seagrass canopy structure: spatially explicit effects on ammonium uptake rates. *Limnol. Oceanogr.* **53** (4), 1531–1539.

MULLARNEY, J.C. & HENDERSON, S.M. 2018 Flows within marine vegetation canopies. In *Advances in Coastal Hydraulics*. World Scientific. https://www.worldscientific.com/worldscibooks/10.1142/10744.

NEPF, H.M. 2012 Flow and transport in regions with aquatic vegetation. *Annu. Rev. Fluid Mech.* **44** (1), 123–142.

PALMER, M.R., NEPF, H.M., PETTERSSON, T.J.R. & ACKERMAN, J.D. 2004 Observations of particle capture on a cylindrical collector: implications for particle accumulation and removal in aquatic systems. *Limnol. Oceanogr.* **49** (1), 76–85.

POGGI, D., PORPORATO, A., RIDOLFI, L., ALBERTSON, J.D. & KATUL, G.G. 2004 The effect of vegetation density on canopy sub-layer turbulence. *Boundary-Layer Meteorol.* **111** (3), 565–587.

REIDENBACH, M.A., KOSEFF, J.R., MONISMITH, S.G., STEINBUCKC, J.V. & GENIN, A. 2006 The effects of waves and morphology on mass transfer within branched reef corals. *Limnol. Oceanogr.* **51** (2), 1134–1141.

VAN ROOIJEN, A.A., LOWE, R., RIJNSDORP, D.P., GHISALBERTI, M., JACOBSEN, N.G. & MCCALL, R. 2020 Wave-driven mean flow dynamics in submerged canopies. *J. Geophys. Res.: Oceans* **125** (3), e2019JC015935.

STRIDE, B., ABOLFATHI, S., ODARA, M.G.N., BENDING, G.D. & PEARSON, J. 2023 Modeling microplastic and solute transport in vegetated flows. *Water Resour. Res.* **59** (5), e2023WR034653.

TAN, W. & YUAN, J. 2022 Drag-related wave–current interaction inside a dense submerged aquatic canopy. *J. Fluid Mech.* **941**, A35.

THOMAS, F. & CORNELISEN, C. 2003 Ammonium uptake by seagrass communities: effects of oscillatory versus unidirectional flow. *Mar. Ecol. Prog. Ser.* **247**, 51–57.

VAN VEELEN, T.J., KARUNARATHNA, H. & REEVE, D.E. 2021 Modelling wave attenuation by quasi-flexible coastal vegetation. *Coast. Engng* **164**, 103820.

VILLANUEVA, R., PAUL, M., VOGT, M. & SCHLURMANN, T. 2017 Vertical biomass distribution drives flow through aquatic vegetation. Presented at the SCACR 2017, Santander.

VREMAN, B., GEURTS, B. & KUERTEN, H. 1997 Large-eddy simulation of the turbulent mixing layer. *J. Fluid Mech.* **339**, 357–390.

WAYCOTT, M., LONGSTAFF, B.J. & MELLORS, J. 2005 Seagrass population dynamics and water quality in the Great Barrier Reef region: a review and future research directions. *Mar. Pollut. Bull.* **51** (1–4), 343–350.

WEITZMAN, J.S., ZELLER, R.B., THOMAS, F.I.M. & KOSEFF, J.R. 2015 The attenuation of current- and wave-driven flow within submerged multispecific vegetative canopies: flow in submerged multispecific canopies. *Limnol. Oceanogr.* **60** (6), 1855–1874.

WHITFIELD, A.K. 2017 The role of seagrass meadows, mangrove forests, salt marshes and reed beds as nursery areas and food sources for fishes in estuaries. *Rev. Fish Biol. Fish.* **27** (1), 75–110.

YSEBAERT, T., YANG, S., ZHANG, L., HE, Q., BOUMA, T.J. & HERMAN, P.M.J. 2011 Wave attenuation by two contrasting ecosystem engineering salt marsh macrophytes in the intertidal pioneer zone. *Wetlands* **31** (6), 1043–1054.

ZELLER, R.B., ZARAMA, F.J., WEITZMAN, J.S. & KOSEFF, J.R. 2015 A simple and practical model for combined wave-current canopy flows. *J. Fluid Mech.* **767**, 842–880.

ZHANG, X., LIN, P. & CHEN, X. 2022*a* Coastal protection by planted mangrove forest during typhoon Mangkhut. *J. Mar. Sci. Engng* **10** (9), 1288.

ZHANG, X., LIN, P., GONG, Z., LI, B. & CHEN, X. 2020 Wave attenuation by Spartina alterniflora under macro-tidal and storm surge conditions. *Wetlands* **40** (6), 2151–2162.

ZHANG, X., LIN, P. & NEPF, H. 2021 A simple wave damping model for flexible marsh plants. *Limnol. Oceanogr.* **66** (12), 4182–4196.

ZHANG, X., LIN, P. & NEPF, H. 2022*b* A wave damping model for flexible marsh plants with leaves considering linear to weakly nonlinear wave conditions. *Coast. Engng* **175**, 104124.

ZHANG, X. & NEPF, H. 2021*a* Wave damping by flexible marsh plants influenced by current. *Phys. Rev. Fluids* **6** (10), 100502.

ZHANG, X. & NEPF, H. 2021*b* Wave-induced reconfiguration of and drag on marsh plants. *J. Fluids Struct.* **100**, 103192.

ZHANG, X. & NEPF, H. 2022 Reconfiguration of and drag on marsh plants in combined waves and current. *J. Fluids Struct.* **110**, 103539.